

Speeding Up PEEC Partial Inductance Computations Using a QR-Based Algorithm

Dipanjan Gope, *Member, IEEE*, Albert E. Ruehli, *Life Fellow, IEEE*, and Vikram Jandhyala, *Senior Member, IEEE*

Abstract—The partial element equivalent circuit (PEEC) approach has been used in different forms for the computation of equivalent circuit elements for quasi-static and full-wave electromagnetic models. In this paper, we focus on the topic of large scale inductance computations. For many problems as part of PEEC modeling, partial inductances need to be computed to model interactions between a large numbers of objects. These computations can be very time and memory consuming. To date, several techniques have been devised to reduce the memory and time required to compute the partial inductance entities, as well as the time required to use them in a circuit analysis compute step. Some of the existing methods use hierarchical compression while some others are based on issues like properties of the inverse of the partial inductance matrix. However, because of inherent limitations, most of these methods are less suitable for PEEC applications. In this paper, we present an approach which is based on the compression of the partial inductance matrix utilizing the QR decomposition of the far coefficients submatrices. The QR-decomposed form is represented as a compressed SPICE-compatible circuit. This yields an efficient and mathematically consistent approach for reducing the storage and time requirements.

Index Terms—Fast solver algorithm, inductance, partial element equivalent circuit (PEEC), QR decomposition.

I. INTRODUCTION

THE accurate modeling of inductive coupling is critical in determining the electrical behavior of high speed, high performance circuits. Consequently, the topic of inductance calculation has gained importance over the years. The approximate analytical formulas employed to this end prior to the use of numerical techniques, e.g., [1], suffer from a lack of accuracy in the solution of complex 3-D structures. The partial element equivalent circuit (PEEC) method was originally conceived as a numerical integral equation-based approach for the large scale accurate computation of inductances in integrated circuits [2]. Progress has been made since then on various aspects of the methodology and new techniques have been developed with the contributions from many researchers. Today, the approach has many applications from inductance calculations to full-wave solution of combined electromagnetic and circuit structures. Recently, the PEEC formulation including the partial

inductances has been generalized for nonorthogonal geometries using quadrilateral and hexahedral cells [3] or triangular discretization, e.g., [4], [5]. The PEEC model, complete with inductive contributions L_p , potential or capacitive contributions (P), resistive part (R), and full-wave specific delays τ , is designated as (L_p, P, R, τ) PEEC. In this paper, we concentrate on the inductance specific applications namely (L_p, R) PEEC.

The PEEC inductive analysis entails the solution of a mostly dense partial inductance matrix $\bar{\mathbf{L}}_p$ consisting of N^2 elements, where N is the number of entities generated by the discretization of test structures. This presents an efficiency bottle-neck caused by the unfavorable $O(N^2)$ scaling in the time and memory requirement for the computation and storage of $\bar{\mathbf{L}}_p$. In addition, since the circuit analysis step corresponds potentially to a matrix solution it requires another $O(N^3)$ step in time. In the past, efforts were made to speed up the evaluation of the integrals without a loss of overall accuracy [2], [6]. However, for large problems, further speedup is desirable. The hierarchical fast multipole method (FMM) was developed to compress the partial inductance matrix first in [7] and later in [8] and [9]. The FMM technique necessitates the construction of an oct-tree hierarchy in 3-D resulting in cubical subregions, which enable the construction and proper utilization of the multipole expansions. An important aspect in this regard is that PEEC employs rigorous integration routines so that the number of unknowns N is greatly reduced by the use of large aspect ratio PEEC cells, where length to width ratios can exceed 1000:1. Cubical subregions are, therefore, less desirable to group the high aspect ratio PEEC cells. The reduction of the cell aspect ratios with the purpose of making it compatible with the FMM hierarchy will generate an increased number of unknowns and is, therefore, counter productive. The other existing techniques attempt to sparsify the $\bar{\mathbf{L}}_p$. Early attempts in sparsification [10] showed that reasonable results could be obtained by omitting inductive couplings. However, it was recognized that the sparsified $\bar{\mathbf{L}}_p$ matrix is no longer positive definite and a method based on pseudo-image returns was devised [11]. This class of method was improved for several years, e.g., [12]. The success of the application of this approach is clearly problem-dependent since it depends on the return path. Other methods were devised like the use of an approximate inverse $\bar{\mathbf{L}}_p^{-1}$ in the circuit solver process [13]. This approach cannot be used for full wave PEEC models since it is based on the inverse of the $\bar{\mathbf{L}}_p$ matrix. Another method which uses a determined return path is given by [14]. Many of these methods were tailored for bus-type structures which usually involve a large number of parallel bars. Another FFT-based approach has been applied to the specific case of on-chip geometries with objects of a similar size [15].

Manuscript received May 4, 2005; revised May 23, 2006.

D. Gope was with the Electrical Engineering Department, University of Washington, Seattle, WA 98195 USA. He is now with the Core CAD Technology Group, Intel Corporation, Santa Clara 95052 USA (e-mail: dipanjan.gope@intel.com).

A. E. Ruehli is with the IBM Research Division, Yorktown Heights, NY 10598 USA (e-mail: ruehli@us.ibm.com).

V. Jandhyala is with the Electrical Engineering Department, University of Washington, Seattle, WA 98195 USA (e-mail: jandhyala@ee.washington.edu).

Digital Object Identifier 10.1109/TVLSI.2007.891089

In this paper, the fast solution algorithm is based on an approach devised originally by Kapur and Long [16] which reduce both the computational complexity of constructing the matrix as well as its solution process. The underlying reason contributing to the dense nature of the partial inductance matrix is that each PEEC inductor interacts with every other PEEC inductor through a current controlled voltage source (CCVS). Therefore, in a system consisting of N PEEC cells, the number of unique CCVS elements is $N(N - 1)$. Using the QR compression scheme, the total number of CCVS elements is reduced to $O(N)$. The entire geometry is first subdivided using a density-balanced binary decomposition which accommodates bounding boxes of any shapes and sizes. This choice of hierarchical binary tree decomposition is particularly attractive for grouping high aspect ratio PEEC cells. The number of CCVS elements required to represent the interaction between partial inductors in well-separated boxes can then be reduced using the QR compression scheme. The compression theory is based on the property of the Green's function kernel embedded in the integral which generates the strength of the CCVS elements. The contribution of this paper is, therefore, as follows:

- application of the QR compression algorithm in PEEC inductive analysis to obtain linear time and memory scaling in terms of increasing number of unknowns;
- representation of the QR compressed partial inductance network using SPICE-compatible net-list.

Section II describes the basics of the PEEC inductive modeling scheme. Section III explains the hierarchy used in the solution process which determines the partial-inductance submatrices amenable to compression. Section IV describes QR matrix compression for each such submatrix. Section V illustrates the circuit representation of the compression technique and the resultant SPICE compatible form. Finally, example results are given in Section VI, followed by the conclusion.

II. PEEC INDUCTANCE MODELING AND COMPRESSION BASICS

The PEEC model is based on a conversion of the sum of all electric field components at a point on an object (2.1) into Kirchhoff's voltage law by an appropriate integration. This leads to a circuit which can be used to model Maxwell's equations for orthogonal or nonorthogonal structures [3]. For the general volume model, the total electric field at a conductor is given by

$$\mathbf{E}_0(\mathbf{r}, t) = \frac{\mathbf{J}}{\sigma} + \frac{\partial \mathbf{A}(\mathbf{r}, t)}{\partial t} + \nabla \phi(\mathbf{r}, t) \quad (2.1)$$

where \mathbf{E}_0 is a potential applied electric field, \mathbf{J} is the current density in the conductors, \mathbf{A} and ϕ are vector and scalar potentials, respectively. The general full-wave volume (L_p , P , R , τ) PEEC model, based on (2.1), includes voltage sources corresponding to the left-hand side and resistances, partial inductances and capacitances corresponding to the right-hand side terms [17]. A unit PEEC cell is illustrated in Fig. 1.

In this paper, we focus on pure inductance modeling, which can be achieved simply by opening the capacitors and thereby neglecting the scalar potential contributions. The complexity of

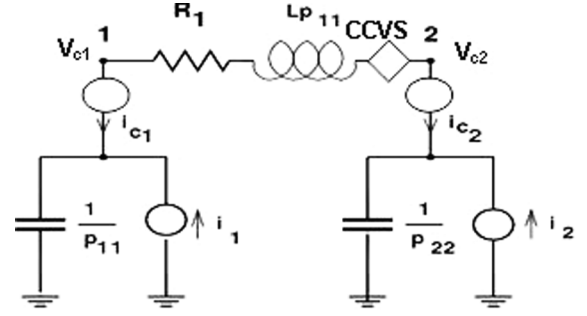


Fig. 1. Basic PEEC circuit, modeling electric field integral equation for a unit PEEC cell. The resistor models the ohmic loss, the inductor and the CCVS model the vector potential, and capacitor and current sources, in parallel, model the scalar potential.

the remaining problem is dominated by the CCVS in Fig. 1. For the i th PEEC cell, the contribution of the CCVS element is given by

$$V_i = \sum_{k=1,2,\dots,n;k \neq i} [\sqrt{-1}] \omega L_{pik} I_k \quad (2.2)$$

where ω is the angular frequency, I_k is the current through the k th inductive cell, and L_{pik} is the mutual inductance obtained by a six-fold integral

$$\begin{aligned} L_{pik} &= \frac{\mu}{4\pi} \frac{1}{a_i a_k} \int_{v_i} \int_{v_k} G(r_i, r_k) dv_i dv_k \\ &= \frac{\mu}{4\pi} \frac{1}{a_i a_k} \int_{v_i} \int_{v_k} \frac{1}{|r_i - r_k|} dv_i dv_k. \end{aligned} \quad (2.3)$$

In (2.3), a represents the cross section of the rectangular volume cell normal to the current direction, v represents the volume, r is the position vector of any point inside the PEEC cell, and G represents the Green's function.

The efficiency bottleneck associated with the traditional PEEC solution involves the time required to compute the coefficients of $N(N - 1)$ CCVS elements by (2.3) and storing them in memory. This also results in the generation of a dense modified nodal analysis (MNA) matrix, the solution of which consumes $O(N^3)$ time. These challenges are addressed by taking advantage of the properties of the Green's function. Consider the interaction between a group of m victim PEEC inductors and another group of n aggressor PEEC inductors. Traditionally, this one-way interaction is modeled by $m \times n$ CCVS elements. However, if the two groups are well-separated in space, the number of circuit elements required to represent the interaction can be reduced by observing that the rank of the interaction matrix is much less than m or n . The associated steps in the entire process are as follows:

- hierarchical grouping of PEEC inductors leading to identification of the compressible interactions;
- QR compression of the interactions identified in the previous step;
- circuit representation of the QR compressed interaction using SPICE-compatible net-list.

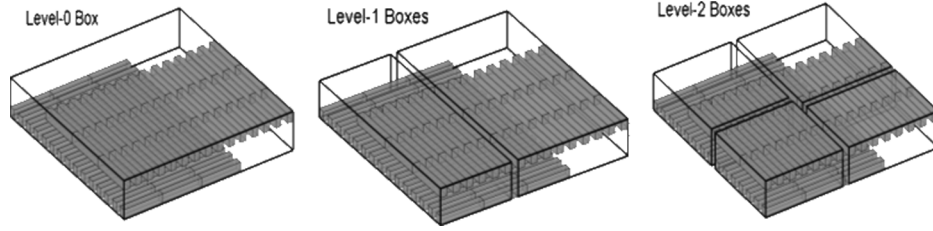


Fig. 2. Hierarchical levels of binary tree geometry decomposition.

III. HIERARCHICAL GROUPING OF PEEC INDUCTORS

In this process, the major consideration is that the boxes generated from hierarchical subdivision should be capable of accommodating the high aspect ratio PEEC cells. There are three main criteria that can be applied independently to yield different hierarchical grouping schemes [18]. They are enumerated as follows with popular choices.

- 1) Degree of decomposition:
 - Binary decomposition: Each cell is divided into two cells.
 - Decomposition into orthants: Each cell is divided into four cells (2-D) or eight cells (3-D).
- 2) Balance of decomposition:
 - Spatial balancing: Each split is equidistant from the cell boundary.
 - Density balancing: Number of particles on each side is equal.
- 3) Definition of cell boundaries:
 - Loose bounds: Boundary derived from split is defined as the cell boundary.
 - Tight bounds: Smallest parallelepiped enclosing cell-points is defined as the cell boundary.

In this application, binary decompositions with density balancing and tight bounds known as tight-bound k -D trees are employed, similar to *IES*³ [16]. Every object is first discretized using coarse volumetric PEEC inductive cells [2], [3]. The smallest hexahedral box that encloses every PEEC inductive filament is called the level-0 box as shown in Fig. 2 for a Manhattan mesh. This is then recursively subdivided into two boxes along the dominant coordinate, which is determined by the maximum size of the parent box in the x -, y -, or z -direction. The position of split is evaluated as

$$x_{\text{split}} = \sum_{i=1}^N \frac{x_i^c}{N} \quad y_{\text{split}} = \sum_{i=1}^N \frac{y_i^c}{N} \quad z_{\text{split}} = \sum_{i=1}^N \frac{z_i^c}{N} \quad (3.4)$$

where N is the number of PEEC cells in the parent box to be split and x_i^c , y_i^c , and z_i^c are the x , y , and z coordinates of the centroid of the i th PEEC cell. It should, therefore, be noted that the split does not necessarily occur through the dominant coordinate midpoint of the parent box, as can be observed from Fig. 2. The entire geometry is decomposed in a binary tree hierarchy, until the number of PEEC cells in the lowest level box does not fall below a threshold value, usually chosen as 20.

Once the binary tree decomposition of the geometry is performed, the box-to-box interactions to be compressed using the

QR-algorithm are identified using a look-up table called the rank-map. Each entry of the look-up table gives an estimate of the expected rank for the interaction and is, therefore, a function of the lengths, widths, and heights of the aggressor and victim boxes and the distance between them. The generation of the look-up table is a one time process, where the rank is determined for the interaction submatrix of a random distribution of basis functions in the source and observer boxes. The dimensions of the boxes and the distance between them are altered by unit increments and a map is generated from the ranks obtained. Simple interpolation techniques are used for estimating ranks wherever specific source-observer cell characteristics are absent. The look-up table is again a function of the tolerance ε_Q in (4.6) specified by the user. Thus, the expected rank r_E for each box-to-box interaction is predicted. The algorithm for identifying the submatrices to be compressed for any given problem is given as follows.

Algorithm 3.1 (Multilevel compressed matrix formation algorithm) Let N_v be the number of PEEC-inductive cells in the victim box and N_a be the number of cells in the aggressor box. Let r_E be the expected rank as predicted by the look-up table for these victim and aggressor boxes then:

Step 1:

If $[\min\{N_v, N_a\} < 4 \times r_E]$

If $[(N_v \times N_a)/(N_v + N_a)] < r_E$

Construct the conventional dense circuit representation for this interaction.

Else

Compress the circuit after constructing the dense representation. The actual rank obtained is r_a .

If $r_a < [(N_v \times N_a)/(N_v + N_a)]$

Keep the compressed circuit. Discard the dense circuit. **Goto Step 3.**

Else

Keep the dense circuit. Discard the compressed circuit. **Goto Step 3.**

Else if $[r_E < 30]$

Construct the compressed circuit from the sampled rows and columns of the dense interaction. The actual rank obtained is r_a .

If [$r_a < 30$]
 Keep the compressed representation. Discard the samples.

Else

Goto Step 2.

Else

Goto Step 2.

Step 2:

Consider the interactions between the children of the victim and aggressor boxes. **Goto Step 1.**

Step 3:

If all interactions have been evaluated, then **Finish.**

Else consider another interaction. **Goto Step 1.**

The application of the algorithm results in the generation of the following two lists of interaction submatrices:

- submatrices which should be represented in the original dense form using traditional PEEC CCVS elements;
- submatrices which are amenable to compression and are handled by the techniques described in Section IV.

IV. QR-BASED COMPRESSION SCHEME

The compression algorithm is based on the observation that the number of degrees-of-freedom for the one-way partial inductance interaction between two well-separated groups of PEEC inductive cells is much smaller than the number of cells in each group. In simple terms, the rows or columns of the interaction submatrix have similar entries due to the smoothness of the $1/r$ kernel in the partial inductance integral. Singular value decomposition (SVD) of this matrix reveals that the magnitude of the singular values falls off rapidly. The same effect can be captured by QR decomposition, which is computationally less expensive. Let $\bar{\mathbf{L}}_{p \times p}^{\text{sub}}$ be the one-way inductive interaction submatrix between p aggressor PEEC cells in one box and m victim PEEC cells belonging to a well-separated second box. We proceed by decomposing the matrix using the modified Gram–Schmidt (MGS) algorithm as part of the QR decomposition of the interaction submatrix. This is done with a user-defined tolerance. Hence, we have

$$\bar{\mathbf{L}}_{p \times p}^{\text{sub}} = \bar{\mathbf{Q}}_{m \times r} \times \bar{\mathbf{R}}_{r \times p} \quad (4.5)$$

where r is the rank of the submatrix for the given tolerance ε_Q such that

$$\frac{\|\bar{\mathbf{L}}_p - \bar{\mathbf{Q}}\bar{\mathbf{R}}\|_2}{\|\bar{\mathbf{L}}_p\|_2} \leq \varepsilon_Q. \quad (4.6)$$

The key aspect is that the number of elements required to represent the interaction submatrix is reduced due to the low rank

r , where $r \ll \min(m, p)$. Consequently, the submatrix storage requirement is reduced. However, if all elements of the dense submatrix need to be computed using (2.3) prior to QR compression, setting up the compressed representation is limited by quadratic time. It has been shown in [16], that linear setup time can be accomplished by constructing the QR representation from some sampled rows and columns instead of explicitly precomputing the entire $\bar{\mathbf{L}}_{p \times p}^{\text{sub}}$ submatrix. The procedure used for computing the sampled rows $\bar{\mathbf{S}}^r$ and sampled columns $\bar{\mathbf{S}}^c$ is considered next. To start with, the first column and the first row are constructed by default as the starting set. Consequently, other columns and rows are selected alternately, based on all previously selected rows and columns according to the following algorithm in linear time.

Algorithm 4.1 (Reduced computation QR): Let

$I_r = \{a, b, c, \dots\}$ be the indices of the k rows and $I_c = \{A, B, C, \dots\}$ be the indices of the k columns chosen already as shown in Fig. 3(a), such that $1 \leq a, b, c, \dots \leq m$; $1 \leq A, B, C, \dots \leq p$ and $a \neq b \neq c \dots$; $A \neq B \neq C \dots$. The $(k+1)$ th row and the $(k+1)$ th column are chosen through the following steps.

Step 1:

k vectors, $v_1^{i=1,2,\dots,k}$ each of length k are constructed as in $[\bar{\mathbf{L}}_p(a, A); \bar{\mathbf{L}}_p(b, A); \bar{\mathbf{L}}_p(c, A); \dots]$, $[\bar{\mathbf{L}}_p(a, B); \bar{\mathbf{L}}_p(b, B); \bar{\mathbf{L}}_p(c, B); \dots] \dots$

Step 2:

$p - k$ vectors, $v_2^{i=1,2,\dots,p-k}$ of length k are constructed from the already existing entries of the nonselected columns which were formed during row selection, as indicated by circles in Fig. 3(a). These vectors are of the form

$$[\bar{\mathbf{L}}_p(a, J); \bar{\mathbf{L}}_p(b, J); \bar{\mathbf{L}}_p(c, J); \dots], \quad \text{where } 1 \leq J \leq p \text{ and } J \neq A \neq B, \dots$$

Step 3:

For each vector v_2^j formed in **Step 2**, where $1 \leq j \leq p - k$, we obtain a value corresponding to

$$\text{MinVal}(j) = \min\left\{\|v_1^1 - v_2^j\|_2, \|v_1^2 - v_2^j\|_2, \|v_1^3 - v_2^j\|_2, \dots\right\}. \quad (4.7)$$

Step 4:

The maximum entry of the MinVal vector obtained in the previous step is obtained and the column corresponding to this maximum value is chosen as the $(k+1)$ th column.

Step 5:

k vectors, $v_3^{i=1,2,\dots,k}$ each of length $k+1$ are constructed as in $[\bar{\mathbf{L}}_p(a, A); \bar{\mathbf{L}}_p(a, B); \bar{\mathbf{L}}_p(a, D); \dots]$, $[\bar{\mathbf{L}}_p(b, A); \bar{\mathbf{L}}_p(b, B); \bar{\mathbf{L}}_p(b, D); \dots] \dots$

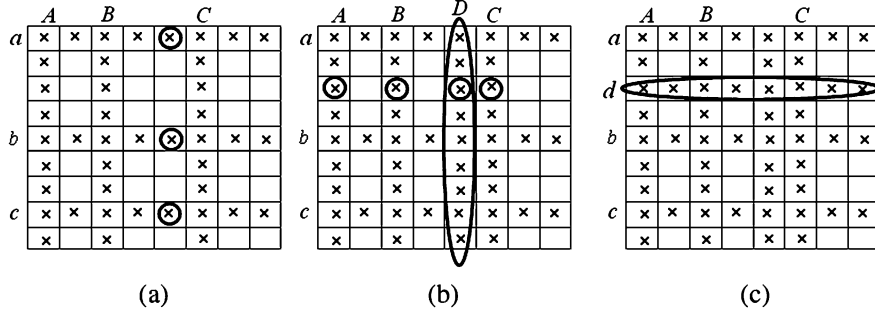


Fig. 3. Selection of new row and column.

Step 6:

$m - k$ vectors, $v_4^{i=1,2,\dots,m-k}$ of length $(k + 1)$ are constructed from the already existing entries of the nonselected rows which were formed during column selection, as indicated by circles in Fig. 3(b). These vectors are of the form

$$[\bar{\mathbf{L}}_p(h, A); \bar{\mathbf{L}}_p(h, B); \bar{\mathbf{L}}_p(h, D); \dots],$$

where $1 \leq h \leq m$ and $h \neq a \neq b \dots$

Step 7:

For each vector v_4^j formed in **Step 6**, where $1 \leq j \leq m - k$, we obtain a value corresponding to

$$\text{MinVal}(j) = \min \left\{ \left\| v_3^1 - v_4^j \right\|_2, \left\| v_3^2 - v_4^j \right\|_2, \left\| v_3^3 - v_4^j \right\|_2, \dots \right\}. \quad (4.8)$$

Step 8:

The maximum entry of the MinVal vector obtained in the previous step is obtained and the row corresponding to this maximum value is chosen as the $(k + 1)$ th row.

From experience, we choose the number of sampled rows and columns to be twice the expected rank of the interaction compute in (4.1). Once the sampled columns and rows are formed as shown, the following steps are used to finally obtain the desired QR form of the matrix in (4.5). First, $\bar{\mathbf{Q}}_{m \times r}$ is formed by the MGS process as

$$\bar{\mathbf{S}}_{m \times s}^c = \bar{\mathbf{Q}}_{m \times r} \bar{\mathbf{R}}_{r \times s}' \quad (4.9)$$

where s is the number of samples chosen. Matrix $\bar{\mathbf{Q}}_{s \times r}'$ is obtained from $\bar{\mathbf{Q}}_{m \times r}$, such that the indices of the chosen rows are the same as the ones used to construct $\bar{\mathbf{S}}^r$ from $\bar{\mathbf{M}}$. Under such conditions

$$\bar{\mathbf{S}}_{s \times p}^r = \bar{\mathbf{Q}}_{s \times r}' \bar{\mathbf{R}}_{r \times p}. \quad (4.10)$$

To solve for $\bar{\mathbf{R}}_{r \times p}$, $\bar{\mathbf{Q}}_{s \times r}'$ is decomposed using MGS into a unitary matrix $\bar{\mathbf{Q}}_{s \times r}''$ and an upper triangular square matrix $\bar{\mathbf{R}}_{r \times r}''$

$$\bar{\mathbf{Q}}_{s \times r}' = \bar{\mathbf{Q}}_{s \times r}'' \bar{\mathbf{R}}_{r \times r}''. \quad (4.11)$$

Using (4.11) and the properties of $\bar{\mathbf{Q}}_{s \times r}''$, (4.10) can be written as

$$\bar{\mathbf{Q}}_{s \times r}''^T \bar{\mathbf{S}}_{s \times p}^r = \bar{\mathbf{R}}_{r \times r}'' \bar{\mathbf{R}}_{r \times p}. \quad (4.12)$$

From (4.12), $\bar{\mathbf{R}}_{r \times p}$ can be extracted by back-substitution since $\bar{\mathbf{R}}_{r \times r}''$ is a square upper triangular matrix.

V. PEEC CIRCUIT INTERPRETATION OF QR REDUCTION

The QR compression described in Section IV will result in a compressed circuit representation of the one-way inductive coupling between a group of aggressor and victim PEEC inductive cells:

$$v = s \bar{\mathbf{L}}_p I. \quad (5.13)$$

The same is true in the time domain where we have $v = \bar{\mathbf{L}}_p (di/dt)$. It should be noted that for the general case the submatrix $\bar{\mathbf{L}}_p$ is not necessarily a square matrix. A circuit illustration of the conventional mutual coupling in one direction is given in Fig. 4.

We notice that the coupling from the aggressor currents, I_1 to I_4 , has been represented as four CCVS elements in each of the three victim partial inductance branches, L_{p55} to L_{p77} . From Section IV it is evident that the mutual coupling between well-separated PEEC inductive cells can be represented as

$$V_{m \times 1} = \bar{\mathbf{Q}}_{m \times r} \bar{\mathbf{R}}_{r \times p} s I_{p \times 1}. \quad (5.14)$$

We want to emphasize that the new interpretations of the compressed partial mutual inductance submatrix, given in this section, do not necessarily obey the usual concepts of conventional partial inductance matrices like symmetry and positive definiteness. However, the external terminal behavior is the same as the original matrix. Here, we simply assume that $\bar{\mathbf{Q}}$ and $\bar{\mathbf{R}}$ are interpreted circuit elements like controlled current or voltage sources and partial inductances. The new compressed partial inductances are called so, since they satisfy the same terminal behavior as their conventional counterparts.

We have some choices for the interpretation of (5.14) as an equivalent circuit. In the first choice, which we call the QL form,

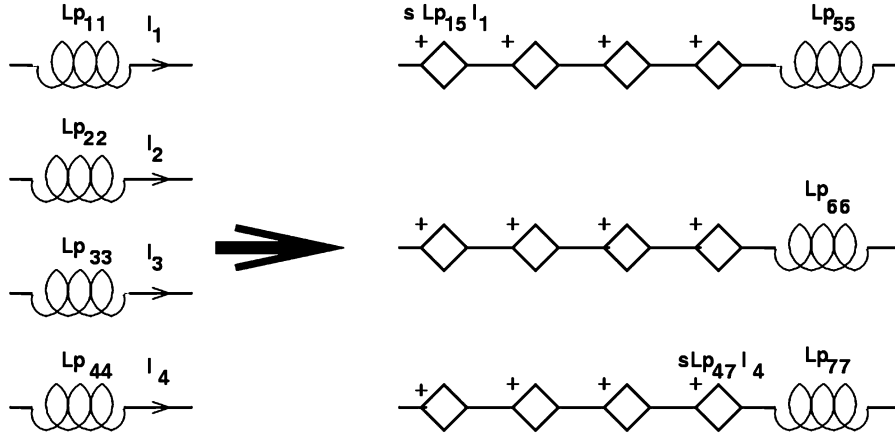


Fig. 4. Circuit interpretation for conventional inductance matrix.

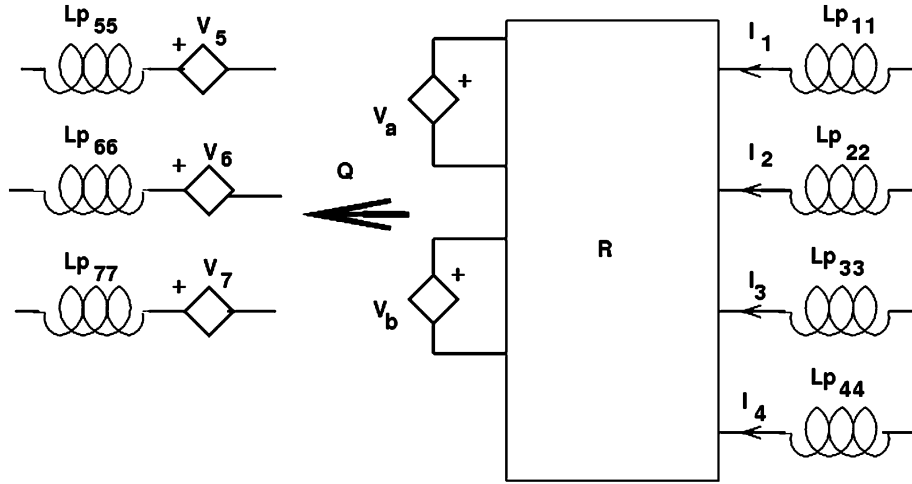


Fig. 5. Circuit interpretation, where R represents partial inductances.

the $\bar{\mathbf{R}}$ part of the QR product is considered to represent the inductances. The resultant equations are given by

$$\begin{bmatrix} V_5 \\ V_6 \\ V_7 \end{bmatrix} = \begin{bmatrix} \alpha_{5a} & \alpha_{5b} \\ \alpha_{6a} & \alpha_{6b} \\ \alpha_{7a} & \alpha_{7b} \end{bmatrix} \begin{bmatrix} L_{p_{a1}} & L_{p_{a2}} & L_{p_{a3}} & L_{p_{a4}} \\ L_{p_{b1}} & L_{p_{b2}} & L_{p_{b3}} & L_{p_{b4}} \end{bmatrix} \begin{bmatrix} sI_1 \\ sI_2 \\ sI_3 \\ sI_4 \end{bmatrix} \quad (5.15)$$

where r intermediate voltage sources are generated from the aggressor currents using the elements of \mathbf{R} , which can, therefore, be treated as partial inductances. The factors α_{ij} which constitute the \mathbf{Q} , map the r voltage sources to the voltage drops in the inductive branches and, therefore, can be represented as SPICE-compatible VCVS. This interpretation is illustrated as an equivalent circuit in Fig. 5. By comparing the equivalent circuit in Fig. 5 with Fig. 4, we see that the conventional coupled sources have been replaced by an equivalent circuit consisting of new controlled sources and partial inductances which are the result of the QR algorithm. Importantly, the number of circuit elements required to represent the interaction has been reduced from mp to $(m+p)r$.

The other circuit representation scheme is the LR option, where \mathbf{R} is interpreted as CCCS elements and \mathbf{Q} represents the partial inductances

$$\begin{bmatrix} V_5 \\ V_6 \\ V_7 \end{bmatrix} = \begin{bmatrix} L_{p_{5a}} & L_{p_{5b}} \\ L_{p_{6a}} & L_{p_{6b}} \\ L_{p_{7a}} & L_{p_{7b}} \end{bmatrix} \begin{bmatrix} \beta_{a1} & \beta_{a2} & \beta_{a3} & \beta_{a4} \\ \beta_{b1} & \beta_{b2} & \beta_{b3} & \beta_{b4} \end{bmatrix} \begin{bmatrix} sI_1 \\ sI_2 \\ sI_3 \\ sI_4 \end{bmatrix} \quad (5.16)$$

Here again, the compressed mutual inductance matrix is symmetric and the properties of the original inductive couplings are maintained. As is evident from Fig. 6, the circuit has a set of r CCCS elements, whose function can be intuitively explained as grouping a large number of currents into an equivalent small number of currents for the particular interaction.

The resultant compressed circuit representation can be used for any type of circuit analysis scheme. Evidently the benefits of the QR compression scheme can be fully exploited in conjunction with an iterative circuit or matrix solver. Even for an iterative solution, two fundamentally different techniques can be applied. For example, a Gauss–Seidel approach is used in

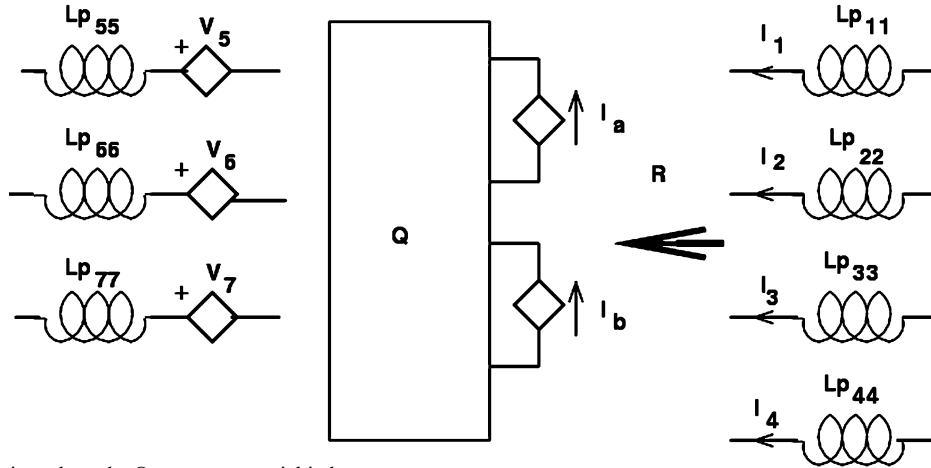


Fig. 6. Circuit interpretation where the Q represents partial inductances.

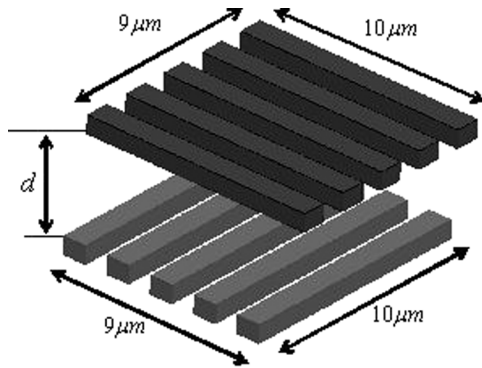


Fig. 7. Test structure to demonstrate the behavior of QR decomposition ranks.

TABLE I
DEMONSTRATION OF CIRCUIT COMPRESSION

distance	N_v	N_o	Uncompressed N_m	rank	N_{occs}	Compressed N_m	Circuit Thinning
5	420	510	214200	36	18360	15120	15%
6	420	510	214200	30	15300	12600	13%
7	420	510	214200	24	12240	10080	10%
10	420	510	214200	18	9180	7560	7.8%
15	420	510	214200	13	6630	5460	5.6%
20	420	510	214200	9	4590	3780	3.9%
30	420	510	214200	9	4590	3780	3.9%
40	420	510	214200	8	4080	3360	3.5%
50	420	510	214200	8	4080	3360	3.5%

[19]. In this approach, convergence is guaranteed since the partitioning is chosen such that the iteration is performed only for inter-block inductive couplings with a coupling factor $\ll 1$. A more conventional approach is to use a preconditioned Krylov subspace iterative solver like the generalized minimum residual (GMRES) method [20] in conjunction with the QR compression, where the complexity for circuit solution is $O(N) \times p \times n_r$, where p is the number of iterations required for convergence and n_r is the number of right-hand sides (RHS).

VI. NUMERICAL RESULTS

In all the following experiments, the error in (4.6) is chosen to be $\varepsilon_Q = 10^{-3}$. We use this tolerance for the QR decomposition as well as the iterative solver residual. The experiments were performed on a 2-GHz machine with 4-GB memory.

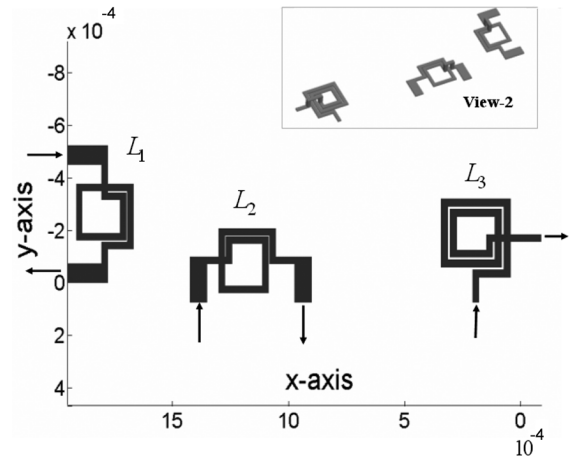


Fig. 8. Structure of three closely placed 3-D on-chip inductors.

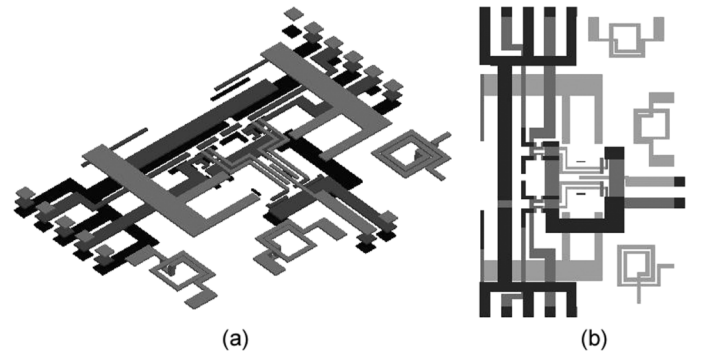


Fig. 9. (a) Three-layer VCO structure with inductor and long interconnects. (b) Layout of the structure.

Example 1: The first example demonstrates the percentage of compression with increasing distances between the victim and observer groups. A bus structure of five interconnects each $10\text{-}\mu\text{m}$ long with a cross section $1\text{-}\mu\text{m} \times 1\text{-}\mu\text{m}$ forms the victim group. A similar five interconnects group, orthogonally placed at a distance, form the observer group, as shown in Fig. 7.

The conductors are discretized using nonorthogonal 3-D-PEEC inductive cells. The mutual interaction between the victim and aggressor groups is given in Table I. N_v is the

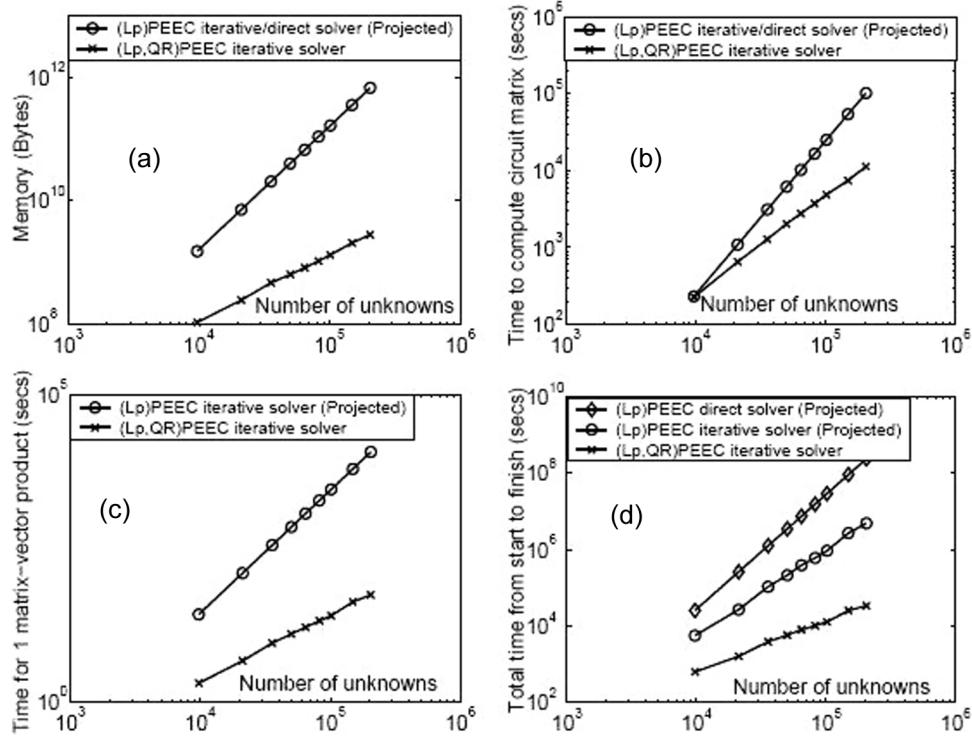


Fig. 10. Efficiency comparison of (QR)PEEC with regular PEEC inductance solver.

number of victim PEEC inductive cells and N_a is the number of aggressor PEEC inductive cells. Uncompressed N_m stands for the number of mutual PEEC inductors in the traditional PEEC format, whereas compressed N_m represents the number of mutual PEEC inductors in the new circuit and N_{CCCS} is the number of current-controlled-current sources, used in the compression scheme, according to Fig. 6. The percentage of circuit thinning represents the reduction of the number of circuit elements in the compressed format as compared to the traditional PEEC circuit.

Example 2: In this example, we consider three closely-spaced on-chip inductors as shown in Fig. 8. The inductors are part of the VCO structure considered in the next example.

The result is a 3×3 inductance matrix for the self and mutual inductance. The inductors are discretized using 6576 unknowns for this example. The memory required in the (QR)PEEC solution is 70 MB. The corresponding time required to generate the compressed circuit elements is 510 s and the time taken to solve the system is 82 s using 68 iterations. The results are matched against those obtained from a commercial solver. The inductances are given as follows in the units of Henries:

$$\begin{bmatrix} 1.383 \times 10^{-9} & 9.63 \times 10^{-12} & -5.27 \times 10^{-12} \\ 9.63 \times 10^{-12} & 9.667 \times 10^{-10} & -1.70 \times 10^{-11} \\ -5.27 \times 10^{-12} & -1.70 \times 10^{-11} & 9.649 \times 10^{-9} \end{bmatrix}$$

Commercial Solver

$$\begin{bmatrix} 1.399 \times 10^{-9} & 8.55 \times 10^{-12} & -4.57 \times 10^{-12} \\ 8.55 \times 10^{-12} & 9.663 \times 10^{-10} & -1.64 \times 10^{-11} \\ -4.57 \times 10^{-12} & -1.64 \times 10^{-11} & 9.641 \times 10^{-9} \end{bmatrix}$$

(QR)PEEC Solver

Example 3: In our final example, the time and memory efficiency of the (QR)PEEC solver is demonstrated for a three-layer VCO structure as shown in Fig. 9.

With this example, we want to demonstrate the behavior of the memory and compute time behavior with the number of unknowns. The memory requirement as a function of the unknowns is plotted in Fig. 10(a). Further, the time required for computing the compressed circuit representation is plotted in Fig. 10(b), while the time required for using the compressed circuit elements in single matrix-vector product is demonstrated in Fig. 10(c). Finally, the total time, which includes the setup phase and the time required for multiple matrix-vector products leading to convergence, is plotted against the number of unknowns in Fig. 10(d).

The numbers for the traditional PEEC approach, namely (LP)PEEC iterative and direct solutions, were obtained by projection from equivalent results for a smaller number of unknowns which would fit in the available memory resources. The improvement in the run-time behavior of the new approach is evident from these experiments.

VII. CONCLUSION

In this paper, the application of the QR compression scheme to PEEC inductive computations is presented. The time and memory requirements are reduced to linear complexity with respect to the number of basis functions. The approach has the advantage that inductive cells with large size aspect ratios can be included. Further, the compression scheme can be represented using a SPICE-compatible equivalent circuit containing far less number of controlled sources as compared to the traditional PEEC approach.

REFERENCES

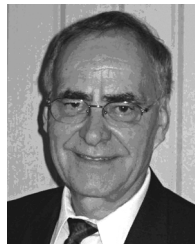
- [1] F. W. Grover, *Inductance Calculations: Working Formulas and Tables*. New York: Dover, 1962.
- [2] A. E. Ruehli, "Inductance calculations in a complex integrated circuit environment," *IBM J. Res. Development*, vol. 16, no. 5, pp. 470–481, Sep. 1972.
- [3] A. E. Ruehli, G. Antonini, J. Esch, J. Ekman, A. Mayo, and A. Orlandi, "Non-orthogonal PEEC formulation for time and frequency domain EM and circuit modeling," *IEEE Trans. Electromagn. Compat.*, vol. 45, no. 2, pp. 167–176, May 2003.
- [4] A. Rong and A. C. Cangellaris, "Generalized PEEC models for three-dimensional interconnect structures and integrated passives of arbitrary shapes," in *Digest Electr. Perf. Electron. Packag.*, 2001, pp. 225–228.
- [5] Y. Wang, V. Jandhyala, and C.-J. R. Shi, "Coupled electromagnetic-circuit simulation of arbitrary-shaped conducting structures," in *Digest Electr. Perf. Electron. Packag.*, 2001, pp. 233–236.
- [6] P. K. Wolff and A. E. Ruehli, "Inductance computations for complex three dimensional geometries," in *Proc. IEEE Int. Symp. Circuits Syst.*, 1981, pp. 16–19.
- [7] M. Kamon, M. J. Tsuk, and J. White, "Fasthenry: A multipole-accelerated 3-D inductance extraction program," in *Proc. Design Autom. Conf.*, 1993, pp. 678–683.
- [8] G. Antonini and A. E. Ruehli, "Fast multipole and multi-function PEEC methods," *IEEE Trans. Mobile Comput.*, vol. 2, no. 4, pp. 288–297, Oct. 2003.
- [9] G. Antonini, "Fast multipole method for time domain PEEC analysis," *IEEE Trans. Mobile Comput.*, vol. 2, no. 4, pp. 275–287, Oct. 2003.
- [10] A. Ruehli, N. Kulasza, and J. Pivnichny, "Inductance of nonstraight conductors close to ground return plane," *IEEE Trans. Microw. Theory Tech.*, vol. 23, no. 8, pp. 706–708, Aug. 1975.
- [11] B. Krauter and L. Pileggi, "Generating sparse partial inductance matrices with guaranteed stability," in *Proc. IEEE Int. Conf. Comput.-Aided Design*, 1995, pp. 45–52.
- [12] M. Beattie and L. Pileggi, "IC analyses including extracted inductance models," in *Proc. Design Autom. Conf.*, 1999, pp. 915–920.
- [13] A. Devgan, H. Ji, and W. Dai, "How to efficiently capture on-chip inductance effects: Including a new element k," in *Proc. IEEE Int. Conf. Comput.-Aided Design*, 2000, pp. 150–155.
- [14] S. C. Chan and K. L. Shepard, "Practical considerations in RLCK crosstalk digital integrated circuits," in *Proc. IEEE Int. Conf. Comput.-Aided Design*, 2001, pp. 598–604.
- [15] H. Hu, D. T. Blauuw, V. Zolotov, K. Gala, M. Zhao, R. Panda, and S. S. Sapathekar, "Inductance simulation using preconditioned-FFT method," *IEEE Trans. Comput.-Aided Design*, vol. 22, no. 1, pp. 49–66, Jan. 2003.
- [16] S. Kapur and D. Long, "IES3: A fast integral equation solver for efficient 3-dimensional extraction," in *Proc. IEEE Int. Conf. Comput.-Aided Design*, 1997, pp. 448–455.
- [17] A. E. Ruehli, "Equivalent circuit models for three dimensional multi-conductor systems," *IEEE Trans. Microw. Theory Techn.*, vol. MTT-22, no. 3, pp. 216–221, Mar. 1974.
- [18] R. J. Anderson, "Tree data structure for n-body simulations," *Siam J. Comput.*, vol. 28, no. 6, pp. 1923–1940.
- [19] A. Ruehli, D. Gope, and V. Jandhyala, "Block partitioned Gauss-Seidel PEEC solver accelerated by QR-based coupling matrix compression techniques," in *Digest Electr. Perf. Electron. Packag.*, 2004, pp. 325–328.
- [20] Y. Saad and M. Schultz, "GMRES: A generalized minimal residual algorithm for solving non-symmetric linear systems," *SIAM J. Sci. Stat. Comput.*, no. 7, pp. 856–869, 1986.



Dipanjan Gope (M'05) received the B.Tech. degree in electronics and electrical communication engineering from the Indian Institute of Technology (IIT), Kharagpur, India, in 2000, and the M.S. and Ph.D. degrees in electrical engineering from the University of Washington, Seattle, in 2003 and 2005, respectively.

He has been a Research Assistant in the Applied Computational Electromagnetics Laboratory, University of Washington and has held a summer internship position at the IBM T. J. Watson Research

Center. Currently, he is with the Design and Technology Solutions Department, Intel Corporation, Santa Clara, CA. His research interests include fast solver algorithms, integral equation formulations, computational electromagnetic solvers for circuit applications, and signal integrity analysis.



Albert E. Ruehli (LF'03) received the Ph.D. degree in electrical engineering from the University of Vermont, Burlington, in 1972.

He has been a member of various projects with IBM including mathematical analysis, semiconductor circuits, and devices modeling, and has been a Manager of a VLSI design and computer-aided design (CAD) Group. Since 1972, he has been with the IBM Thomas J. Watson Research Center, Yorktown Heights, NY, where he is currently a Research Staff Member in the Electromagnetic Analysis Group. He is the editor of two books *Circuit Analysis* (North-Holland, 1986) and *Simulation and Design* (North-Holland, 1987) and he is an author or coauthor of over 100 technical papers. He has given talks at universities including keynote addresses and tutorials at conferences, and has organized many sessions.

Dr. Ruehli has served in numerous capacities for the IEEE. In 1984 and 1985, he was Technical and General Chairman, respectively, of the ICCD International Conference. He has been a member of the IEEE ADCOM for the Circuit and System Society and an Associate Editor for the IEEE TRANSACTIONS ON COMPUTER-AIDED DESIGN OF INTEGRATED CIRCUITS AND SYSTEMS. He was a recipient of the IBM Research Division for IBM Outstanding Contribution Awards in 1975, 1978, 1982, 1995, and 2000, the Guillemin-Cauer Prize Award for his work on waveform relaxation in 1982, a Golden Jubilee Medal in 1999, both from the IEEE CAS Society, a Certificate of Achievement from the IEEE EMC Society for inductance concepts and the partial element equivalent circuit (PEEC) method in 2001, and the 2005 Richard R. Stoddart Award from the IEEE EMC Society for outstanding technical performance. He is a member of SIAM.



Vikram Jandhyala (M'00–SM'03) received the B.Tech. degree in electrical engineering from the Indian Institute of Technology (IIT), Delhi, India, in 1993, and the M.S. and Ph.D. degrees from the University of Illinois, Urbana-Champaign, in 1995 and 1998, respectively.

As part of his graduate work, he codeveloped the steepest descent fast-multipole method for rapid simulation of a large class of EM problems. From 1998 to 2000, he was a Research and Development Engineer with the Ansoft Corporation, Pittsburgh, PA. He was

involved in the acceleration of Ansoft's integral-equation solvers, and co-developed a fast multipole-based extraction tool in Ansoft's Q3-D versions released in 1999 and 2000. Since 2000, he has been an Assistant Professor with the Electrical Engineering Department, University of Washington, Seattle, where he directs the Applied Computational Electromagnetics Laboratory. His research interests and projects include several areas of computational electromagnetics, including fast solvers and integral-equation formulations in the frequency and time domains, high-speed circuits and devices, coupled multiphysics simulation, novel materials, and propagation. He has visiting research status with the Lawrence Livermore National Laboratories. He has authored or coauthored over 70 journal and conference papers. He is a full elected member of the International Scientific Radio Union (URSI) Commission B. He has served as a reviewer for several IEEE journals and conferences and national and international proposal panels. He is on the Technical Program Committee of the IEEE Design Automation Conference and the IEEE Antennas and Propagation Society (IEEE AP-S) Symposium.

Dr. Jandhyala was a recipient of the 2001 National Science Foundation (NSF) Career Grant, a 1998 Outstanding Graduate Research Award presented by the University of Illinois, and the IEEE Microwave Graduate Fellowship for 1996–1997.